

Experimental and numerical study on soot formation in laminar diffusion flames of biodiesels and methyl esters

B. Tian^{a,b}, A. Liu^{c,d}, C. T. Chong^{e,f}, L. Fan^a, S. Ni^a, J.-H. Ng^g, S. Rigopoulos^d, K. H. Luo^c, S. Hochgreb^a

^a*Department of Engineering, University of Cambridge, Trumpington Street, CB2 1PZ Cambridge, United Kingdom*

^b*College of Engineering and Technology, University of Derby, Markeaton Street, DE22 3AW Derby, United Kingdom*

^c*Department of Mechanical Engineering, University College London, Torrington Place, London WC1E 7JE, United Kingdom*

^d*Department of Mechanical Engineering, Imperial College London, Exhibition Road, London SW7 2AZ, United Kingdom*

^e*China-UK Low Carbon College, Shanghai Jiao Tong University, Lingang, Shanghai, 201306, China*

^f*School of Mechanical Engineering, Faculty of Engineering, Universiti Teknologi Malaysia, 81310 Skudai, Johor, Malaysia*

^g*Faculty of Engineering and Physical Sciences, University of Southampton Malaysia, 79200 Iskandar Puteri, Johor, Malaysia*

Abstract

Biodiesel and blends with petroleum diesel are promising renewable alternative fuels for engines. In the present study, the soot concentration generated from four biodiesels, two pure methyl esters, and their blends with petroleum diesel are measured in a series of fully pre-vapourised co-flow diffusion flames. The experimental measurements are conducted using planar laser induced-incandescence (LII) and laser extinction optical methods. The results show that the maximum local soot volume fractions of neat biodiesels are 24.4% - 41.2% of pure diesel, whereas the mean soot volume fraction of

Email address: anxiong.liu@ucl.ac.uk (A. Liu)

neat biodiesel cases was measured as 11.3% - 21.3% of pure diesel. The addition of biodiesel to diesel not only reduces the number of inception particles, but also inhibits their surface growth. The discretised population balance modelling of a complete set of soot processes is employed to compute the 2D soot volume fraction and size distribution across the tested flames. The results show that the model also demonstrates a reduction of both soot volume fraction and primary particle size by adding biodiesel fuels. However, it is not possible to clearly determine which factors are responsible for the reduction from the comparison alone. Moreover, analysis of the discrepancies between numerical and experimental results for diesel and low-blending cases offers an insight for the refinement of soot formation modelling of combustion with large-molecule fuels.

Keywords: Biodiesel, Soot, Laser induced incandescence, soot model

1. Introduction

1 Soot is a known hazardous pollutant resulting from the combustion of
2 carbon fuels; understanding how to suppress its formation via the addition
3 of biodiesel or methyl ester (ME) surrogates is important for the development
4 of low-emission combustion techniques. Biodiesels are typically mixtures of
5 methyl esters (MEs) of long chain fatty acids, which are produced via the
6 transesterification process of triglycerides and short-chain alcohols [1]. The
7 presence of the ester moiety in the molecules of the biodiesel leads to lower
8 soot formation during its combustion compared with conventional petroleum
9 diesel [2].

10 Soot measurements have been made in a number of well-controlled lab-

11 scale flames and reactors, which can act as test beds for soot propensity of
12 biofuel blends. Tran et al. [3] investigated the sooting tendency of soybean
13 biodiesel and petroleum diesel blends using LII in a wick-fed lamp, showing
14 that the addition of biodiesel produced significantly lower soot [4].

15 Abboud et al. [5] evaluated the soot reduction effect of the addition of
16 methyl decanoate (MD), a biodiesel surrogate to diesel in coflow diffusion
17 flames. A similar method was used by Gao et al. [6] to investigate the
18 chemical mechanism and soot reduction effects of dibutyl ether (DBE) in ad-
19 dition to MD. Kholghy et al. [7] analysed the chemical properties of the ester
20 bond for soot evolution and morphology in the flame with a biodiesel sur-
21 rogate comprising 50%/50% molar blend of n-decane and methyl-octanoate.
22 Merchan-Merchan et al. [8] measured the soot volume fraction (f_v) profiles
23 in a pre-vapourised diffusion flame of biodiesels, and evaluated the effect
24 of blending ratio (with diesel) and oxygen concentration in the co-flow on
25 soot formation. The same group [9] also investigated the evolution profiles
26 of the morphological properties of soot in pre-vaporised diffusion flames of
27 three types of biodiesel. Lemaire *et al.* [10] extensively studied the soot and
28 PAH formation in turbulent spray flame of diesel, diesel surrogate, rapeseed
29 methyl ester (RME) and different RME surrogates, and concluded that the
30 soot volume fraction measured in a pure RME flame was around 16% that of
31 pure diesel. Das *et al.* [11] investigated the effect of the double bonds on the
32 sooting properties of esters and produced insights regarding the strong de-
33 pendence of the sooting tendencies of esters on their chemical structure and
34 on their unsaturation degree. Chong *et al.* [12] compared the propensity of
35 soot formation between diesel and waste cooking oil over both a laminar pool

36 flame and a prevapourised diffusion flame. These studies have expanded the
37 understanding of soot formation and properties in pre-vapourised diffusion
38 flames with biodiesel and MEs. In all previous studies cited above, except
39 for our recent study on diesels and cooking oils [13], the fuel was diluted
40 with N₂ [6–9, 14] or argon [5] to improve flame stability during experiments.
41 However, the inert carrier gas may affect the soot formation and yield in
42 these types of flames [15].

43 In the present study, neat undiluted fuel vapour is delivered to the fuel
44 tube to the burner nozzle. Due to the absence of a carrier gas, however,
45 the overall flow velocity of the vapour in the fuel tube is kept very low (\leq
46 0.8 cm/s), so as to minimise flame hydrodynamic stability. In addition, the
47 inherent stability issue of vapour feeding rate was solved by: 1) increasing
48 the volume of the vapour delivery tubing; 2) using a precisely controlled
49 evaporating system. The undiluted flames provide information on the soot
50 formation in neat biodiesel vapour flames, which can serve as important ref-
51 erences for engine emission studies and as validation targets for modelling.
52 Four different actual methyl ester biodiesels derived from carotino red palm
53 (CP), rice bran (RB), duck fat (DU), goose fat (GO), and their blends with
54 petroleum diesel are investigated. Diesel and two pure methyl esters are
55 tested as references. The soot volume fraction (f_v) in tested flames is then
56 measured using extinction-calibrated LII [16] and corrected for signal trap-
57 ping effects using the algorithm developed in [17].

58 Modelling of soot formation and oxidation of biomass-derived fuels is
59 a considerable challenge due to the complexity of chemical reactions and
60 soot formation pathways in the biodiesel fuels. The present study not only

61 presents new experimental data on the behaviour soot from selected fuels,
62 but also uses a comprehensive kinetic mechanism developed for a large vari-
63 ety of fuels related to diesel and biodiesel [18] to simulate the pyrolysis and
64 combustion of fuel blends. A discretised population balance method, consid-
65 ering a complete set of processes of soot evolution [19], is coupled with the
66 reacting flow to model soot formation in the combustion of biodiesel blends.
67 The experimental setup and model details are described forthwith.

68 **2. Experiment**

69 *2.1. Fuels and flame*

70 The tested fuels in the present study are all methyl esters (ME) produced
71 from plant oil or animal fat feedstocks via the transesterification process.
72 The feedstocks used are carotino red palm oil (CP), rice bran (RB), duck fat
73 (DU) and goose fat (GO). The two methyl esters tested are methyl laurate
74 (ML) and methyl myristate (MM). European low-sulfur diesel which had
75 been extensively studied on sooting tendency [10, 13, 20] is tested as a base-
76 line. The composition of different types of biodiesel is measured using a gas
77 chromatograph (GC, Agilent 7620A) based on the EN14103 standard, and
78 listed in Table 1. The measured average formula for CP, RB, DU and GO
79 are: $C_{18.7}H_{36.9}O_{2.0}$, $C_{18.6}H_{36.9}O_{2.0}$, $C_{18.3}H_{36.5}O_{2.0}$ and $C_{18.5}H_{36.6}O_{2.0}$, respec-
80 tively. The formula for ML and MM are $C_{13}H_{26}O_2$ and $C_{15}H_{30}O_2$. It should
81 be clarified that saturated C18 or C19 methyl esters (methyl palmitate and
82 methyl stearate, respectively) could be more suitable than C13 and C15 for
83 a direct comparison with the tested biofuels. However, their high boiling
84 temperature and melting points rendered these substances very difficult to

85 vapourise with the current set up without further heating. For safety rea-
86 sons, this was not feasible in the present study. All biodiesels tested contain
87 about 11% (mass fraction) of oxygen. However, the unsaturation levels of
88 the two types of animal fat derived biodiesel (DU and GO) are much lower
89 than plant-based biodiesel (CP and RB), as listed on Table 1. A previous
90 study [17] on unsaturation suggests that the soot yields of CP and RB are
91 higher than DU and GO. In contrast, the two fully-saturated methyl esters
92 of ML and MM are expected to produce the least soot.

93 A diagram of the pre-vapourised diffusion burner is shown in Fig. 1. The
94 liquid fuels are injected into the vaporising system via a syringe pump (NE-
95 300 Just Infusion Syringe Pump, with accuracy Within $\pm 1\%$ of the displayed
96 value). The mass flow rates of fuels are regulated based on a previous study
97 of the mass consumption rates of the liquid fuels in a buoyancy-induced lam-
98 inar pool flame as described in [12, 17]. The values are selected as 0.119
99 g/min for diesel, 0.116 g/min for CP, 0.104 g/min for RB, 0.111 g/min for
100 DU, 0.094 g/min for GO, 0.130 g/min for ML and 0.115 g/min for MM. All
101 values above are with $\pm 1\%$ instrumental uncertainty. Nevertheless, the esti-
102 mated heat release rates for all the tested neat cases are within $\pm 15\%$ of the
103 mean. A co-flow of air at 0.18 m/s is used to stabilise the diffusion flame. The
104 fuel delivery line is heated using electrical heating tapes (OMEGA STH102
105 series). The temperature of the tapes is controlled by two closed-loop tem-
106 perature controllers, while a thermometer is used to monitor the temperature
107 of the heating tape at the inlet of the system, which is denoted as T_1 . The
108 temperatures in the middle and the outlet of the system are denoted as T_2
109 and T_3 respectively. During the tests, T_1 , T_2 and T_3 are maintained constant

	CP	RB	DU	GO	ML	MM
C12:0	0.000	0.000	0.000	0.000	1.000	0.000
C14:0	0.003	0.004	0.009	0.004	0.000	1.000
C16:0	0.139	0.216	0.317	0.268	0.000	0.000
C18:0	0.602	0.431	0.565	0.588	0.000	0.000
C18:1	0.172	0.321	0.110	0.131	0.000	0.000
C18:2	0.068	0.012	0.000	0.009	0.000	0.000
C18:3	0.016	0.016	0.000	0.000	0.000	0.000
Unsat.	0.356	0.394	0.110	0.149	0.000	0.000
Avg. C	17.71	17.55	17.33	17.45	12.00	14.00
Chain						
MW^a	293.2	291.0	288.4	290.0	214.0	242.0
ΔH^b	40.6	37.50	39.4	39.4	38.02	39.03
Y_C	0.77	0.77	0.76	0.76	0.73	0.74
Y_H	0.13	0.12	0.13	0.13	0.12	0.12
Y_O	0.11	0.11	0.11	0.11	0.15	0.13
X_C	18.7	18.6	18.3	18.5	13	15
X_H	36.7	36.3	36.4	36.6	26	30
X_O	2	2	2	2	2	2

a: units: g/mol; b: units: MJ/kg

Table 1: Properties and compositions of biodiesel fuels. CP: carotino red palm oil biodiesel. RB: rice bran biodiesel. GO: goose fat biodiesel. DU: duck fat biodiesel. ML: methyl laurate. MM: methyl myristate. Top section: Composition (mole fraction) of biodiesels measured using GC. C12:0 means 12 carbon atoms in the main chain of fatty acid with zero double C = C bonds. Bottom section: Properties and elemental mass percentage of biodiesels. The degree of unsaturation is calculated by multiplying the mole fraction of each species times the associated number of C = C double bonds. Heating values ΔH of CP are from [4, 21]; heating value of yellow grease biodiesel from [4] is used as values of DU and GO; values for RB are from [22, 23]; values for ML and MM are from the NIST website [24, 25]. The mass fractions and average molecular formula are denoted by Y and X , respectively.

110 at 520 ± 30 °C, 470 ± 30 °C and 400 ± 30 °C, respectively. As the boiling
 111 point of the fuels are below 400 °C [4], the temperature is sufficiently high
 112 for a full vapourisation. The fuel vapourisation line is designed to achieve
 sufficiently long residence times (≥ 3 min) to ensure full evaporation.

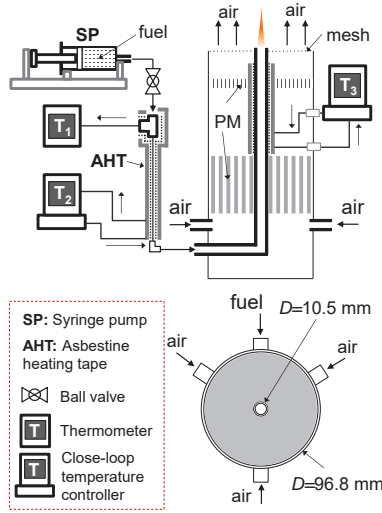


Figure 1: Schematic of the co-flow diffusion flame.

113

114 2.2. LII measurement and calibration

115 The planar 2D LII measurements are performed using a setup similar to
 116 that in Ref. [17], in which the measured LII signal is quantitatively calibrated
 117 via absorption, with correction for signal-trapping. The full details of the
 118 optimisation, calibration and correction procedure of the signals can be found
 119 in Ref. [17].

120 2.3. SEM sampling

121 Soot particle samples are collected by using the thermophoretic deposi-
 122 tion method used in [9]. The soot produced from the flames were collected

123 by using a pre-cooled quartz plate at about 0 °C (76.2×25.4×1.0 mm). By
124 inserting the plate in the flame at the fixed HAB of 15 mm for approximately
125 2 s, soot particles are deposited on the plate driven by the temperature gra-
126 dient between the cold surface and the hot environment. The surface growth
127 of particles can be quickly quenched, and the particles tend to freeze on the
128 surface [9]. Previous studies using quartz plates to collect soot samples show
129 that the collection time does not significantly influence the soot character-
130 istics [26, 27]. The primary soot particle size is analysed using a scanning
131 electron microscope (SEM) (LEO GEMINI 1530VP FEG-SEM) system.
132 From the SEM images, the distribution of the primary particle size is deter-
133 mined and fitted using lognormal distributions based on the measurement of
134 100 random primary particles.

135 **3. Soot modelling**

136 The simulation employs a semi-detailed kinetic mechanism [18] for the
137 pyrolysis and combustion of a large variety of gasoline and diesel fuels in
138 premixed flames, where 249 chemical species and 8153 combined chemical
139 reactions are considered. This mechanism was initially developed based on
140 hierarchical modularity and then improved via the validation with a vast
141 amount of experimental data on the laminar flame speeds of hydrocarbon
142 and oxygenated fuels. In the mechanism, long-chain alkanes, alkenes and
143 a small fraction of aromatic hydrocarbons represent the composition of the
144 diesel, while saturated and non-saturated methyl esters represent the compo-
145 sition of biodiesel fuels. In addition, aromatic hydrocarbons are also involved
146 in the chemical kinetics to model the nucleation process in the soot forma-

147 tion. Therefore, the mechanism cited in the supplementary material in Ref.
 148 [18] is integrated to deal with the chemical reactions of diesel and biodiesel
 149 surrogates, as well as the soot formation precursors.

150 According to [28, 29], the diesel fuel is approximated as a mixture of long-
 151 chain alkanes and alkenes, with a small fraction of aromatic hydrocarbons.
 152 The four biodiesel surrogates are assumed to be a mixture of a long-chain
 153 alkane (n-hexadecane, n-C₁₆H₃₄), a alkene (1,4-hexadiene, HXD14), a satu-
 154 rated methyl ester (MD) and a non-saturated methyl ester (methyl trans-
 155 3-hexenoate, MH3D) [30]. However, some species are absent in the mecha-
 156 nism [18], and are thus substituted by other substances of similar chemical
 157 structures. Therefore, the approximate composition of the diesel fuel and
 four biodiesel surrogates used in the simulation is shown in Tables 2 and 3.

Table 2: Setup of composition of diesel (mass %)

Composition	Refs. [28, 29]	Present
C ₁₀ H ₂₂	5.6	7.6
C ₁₂ H ₂₆	20.9	20.9
C ₁₄ H ₃₀	26.0	26.0
C ₁₆ H ₃₄	16.6	30.4
C ₁₈ H ₃₆	15.8	—
C ₆ H ₁₂	3.7	3.7
C ₁₀ H ₁₈	6.4	6.4
C ₇ H ₈	5.0	5.0

158

159 The soot model involves the processes of nucleation by PAH dimeri-
 160 sation, surface growth by the HACA mechanism [31], PAH condensation
 161 and coagulation of spherical particles and fractal aggregates. Naphthalene
 162 (A2), phenanthrene (A3), pyrene (A4) are used to model PAH dimerisation,
 163 with sticking efficiencies 0.001, 0.015, 0.025 respectively [32]. Reversibility

Table 3: Setup of composition of biodiesel surrogates (mole %)

Ref. [30]	Present	CP	RB	DU	GO
MD: C ₁₁ H ₂₂ O ₂	C ₁₁ H ₂₂ O ₂	53.09	54.98	52.99	52.84
MH3D: C ₇ H ₁₂ O ₂	C ₅ H ₈ O ₂	1.37	2.56	0.88	1.05
	C ₈ H ₁₄ O ₂	2.74	5.13	1.76	2.10
Hexadecane: C ₁₆ H ₃₄	C ₁₆ H ₃₄	40.23	36.41	44.37	43.76
HXD14: C ₆ H ₁₀	C ₅ H ₈	1.28	0.46	0.00	0.13
	C ₇ H ₁₂	1.28	0.46	0.00	0.13

164 of dimerisation is not considered. The collision kernel in the coagulation
 165 term for the free molecular and continuum regimes is described according to
 166 Vemury and Pratsinis [33]. Therefore, the coagulation rate is dependent on
 167 particle size and temperature. The empirical parameters therein were cali-
 168 brated based on ethylene diffusion flames [19] using the gas-phase chemistry
 169 by Blanquart *et al.* [34]. More details on the model can be found in [19].

170 4. Results and discussion

171 Figure 2 presents the measured and modelled spatial distribution of the
 172 soot volume fraction, f_v , for the case of a neat diesel flame (D100) from
 173 HAB = 4 mm to 32 mm. The D100 flame is a sooting flame, and unburnt
 174 soot is emitting from the flame tip. The probe volume does not cover the
 175 whole flame due to the limited size of the laser sheet. However, the maximum
 176 soot volume fraction zone is captured. Both measured and model patterns
 177 of the sooting zone indicate a coincidence of the highest soot zone forming

178 region on the inside of the high temperature zone. The model results show a
 179 significantly broader distribution compared to the very thin measured soot
 180 production zone.

181 The inception of soot takes place around the intersection between the fuel
 182 and air streams at the burner exit, and the maximum soot volume fraction
 183 $f_{v,m}$ appears near the reaction zone at the interface of fuel and air, at between
 184 20 and 25 mm HAB (22.0 mm for measured data and 24.5 mm for model).
 185 The predicted maximum soot volume fraction obtained by the simulation
 186 (6.9 ppm) is only 52% of the experimentally measured value of 13 ppm).
 The sooting propensity of biodiesels and methyl esters was investigated in

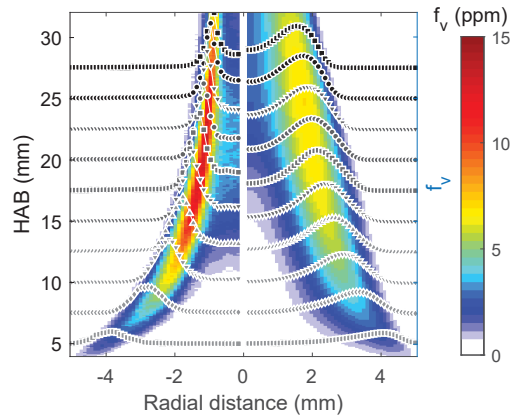


Figure 2: Measured (left) and modelled (right) f_v in D100 flame from HAB = 4 to 32 mm. Dotted lines show profiles plotted in steps of 5 mm HAB.

187

188 six series of cases (from CP to MM). The tested cases are noted by the two
 189 initial letters of the biofuel and the percentage by mass used in the mixture,
 190 e.g. CP20 refers to 20% by mass in carotino red palm oil biodiesel. The
 191 results of all tested cases are shown in Fig. 3. The tested biodiesel cases
 192 denoted as CP, RB, DU and GO are shown in the four rows. Both measured

193 and simulated f_v map of each case are shown in each sub-figure. However,
 194 due to the lack of validated reaction mechanism, the flames of ML and MM
 195 are not modelled, hence only the measured data of the two methyl esters
 196 are shown in Fig. 3 (bottom line of sub-figures). For cases with blending
 197 ratio $r_b \leq 60\%$ of biodiesel, the visible flame height is not well-defined, as
 198 the unburnt soot emits from the flame tips. In contrast, when $r_b \geq 80\%$,
 199 the soot no longer emits from the flame tip, which means all soot is oxidised
 200 across the flame.

201 Measurements show a dramatic drop in the observable height where soot
 202 is detected, r_b , from 60% to 80%. However, this behaviour is not repro-
 203 duced well by the simulation. For all four cases of biodiesel blends, when
 204 $r_b \geq 80\%$, the calculated maximum heights where soot is found are sig-
 205 nificantly larger than experimental measurements. The behaviour of the
 206 sooting region height can be explained using the variation in the stoichio-
 207 metric mixture fraction Z_{st} of the diffusion flames, which can be evaluated
 208 by $Z_{st} = (Y_{ox,0}/S)/(Y_{fu,0} + Y_{ox,0}/S)$, where $Y_{ox,0}$ is the mass fraction of O_2
 209 in the oxidiser side and $Y_{fu,0}$ is the mass fraction of fuel in the fuel stream,
 210 S is the stoichiometric mass ratio of O_2 to fuel. The calculated Z_{st} for D100
 211 is 0.0155, 0.0180 ± 0.0005 for all neat biodiesel, 0.0191 for ML and 0.0186 for
 212 MM. Higher Z_{st} suggests a location of the isosurface towards the fuel side,
 213 thus rendering the flame and sooting zone thinner. Values for the maximum
 214 soot volume fraction $f_{v,m}$ in each flame series are shown in Fig. 4. Both
 215 experiment and simulation show a decrease in $f_{v,m}$ with increasing r_b . Pure
 216 diesel yields the highest f_{vm} due to the presence of aromatic hydrocarbons
 217 and zero bound oxygen. In all neat and blended cases, two biofuels CP and

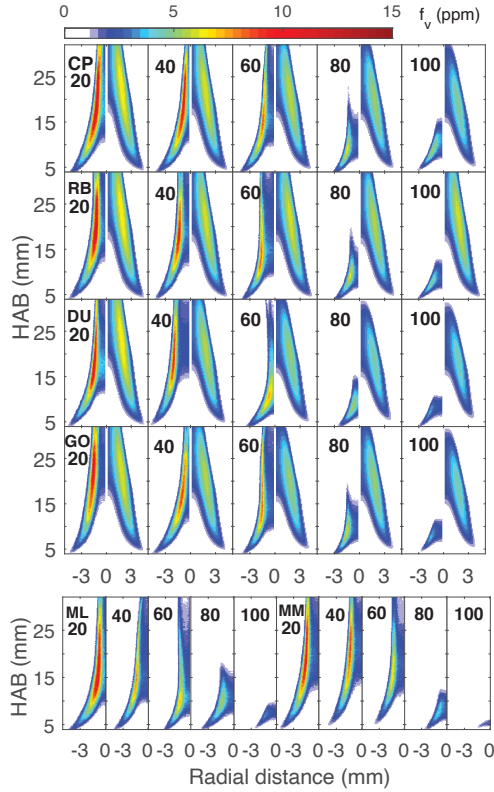


Figure 3: Upper: measured and modelled f_v for each test case. Measurements (left panels), models (right panels) for each fuel and % by mass addition. Bottom: measured f_v for ML and MM cases.

218 RB, which are derived from plant oil with higher unsaturation degree (UD)
 219 yield higher $f_{v,m}$ than DU and GO. Considering that the oxygen mass frac-
 220 tion of the tested biodiesels are almost identical, the result indicates that the
 221 UD is a key factor for soot yield, as observed in [17] for other fuels. This
 222 finding is in consistency with Das *et al.*'s study [11]. Not surprisingly, ML
 223 and MM produce lowest $f_{v,m}$, in which the values in ML100 and MM100 are
 224 24.4% and 14.2% of D100, owing to the fact that they are fully saturated
 225 and with higher oxygen mass fraction as indicated in Table 1. Although

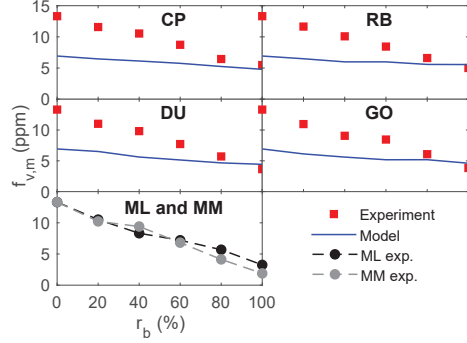


Figure 4: Measured and modelled $f_{v,m}$ as a function of biodiesel volume fraction.

226 the model does predict correctly a decrease in $f_{v,m}$ with r_b for all biodiesels,
 227 the rate of change is not well predicted. However, the very low maximum
 228 soot values for all neat biodiesels are very well predicted. A database of
 229 measured and modelled f_v distributions (data-readable TIFF figure) for all
 230 tested cases is presented as supplementary data. Previous studies show that
 231 the biodiesels reduce soot formation by both the displacement of aromatic
 232 species with long-chained esters, as well as the presence of oxygen [10, 35].
 233 The maximum soot volume fraction, $f_{v,m}$, obtained, per unit carbon for the
 234 tested neat fuel cases is shown in Fig. 5. The value obtained per unit carbon
 235 for diesel is about 2.5 times that of biodiesels and 5 times that of pure methyl
 236 esters.

237 A reasonable, if imperfect, measure of the total soot formation propen-
 238 sity can be constructed using an integrated total mean soot volume fraction
 239 $\bar{f}_{v,int}$ in the flames over the detectable region from $HAB = 0$ to 32 mm, so
 240 that $\bar{f}_{v,int} = (\frac{1}{\pi R^2 H}) \int_0^H \int_0^R 2\pi r f_v(r) dr dz$, where R is the radius of the fuel
 241 tube and $H = 32$ mm. The measured values of $\bar{f}_{v,int}$ for diesel, CP, RB,
 242 DU and GO biodiesels are 2.18, 0.60, 0.44, 0.32 and 0.33 ppm respectively,

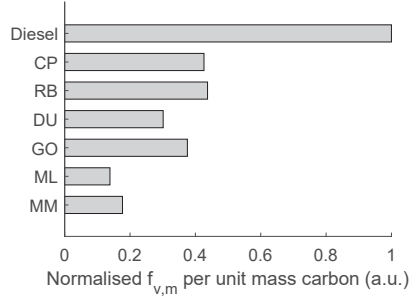


Figure 5: Normalised maximum soot volume fraction $f_{v,m}$ per unit of carbon consumed.

243 while the modelled values are 1.47, 0.75, 0.87, 0.65 and 0.70 ppm, a signifi-
 244 cant discrepancy, which is larger for the biodiesel cases. An area-based mean
 245 soot volume fraction can be defined as $\bar{f}_v = (\frac{1}{\pi R^2 H}) \int_0^R 2\pi r f_v(r) dr$ for each
 246 area, to identify the regions of higher discrepancy. The mean soot volume
 247 fractions as a function of HAB \bar{f}_v of all neat cases are plotted in Fig. 6.
 For the neat biodiesel cases, the predicted values of \bar{f}_v are commensurate

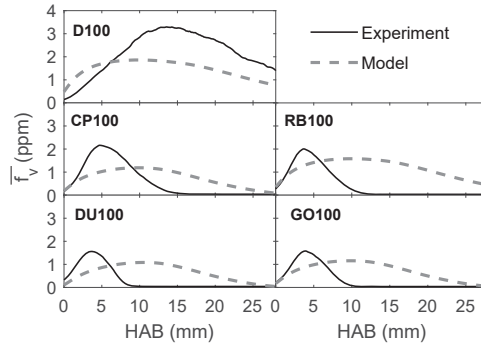


Figure 6: Measured and modelled area weighted mean soot volume fraction $\frac{1}{\pi R^2} \int_0^R 2\pi r f_v(r) dr$ in unblended cases. R is the radius of the fuel tube.

248

249 with the measurements, but the extent of the measurements is confined to
 250 a much narrower region, as expected from 3. The SEM measured particle
 251 size and corresponding lognormal fits for all neat cases are shown in Fig.

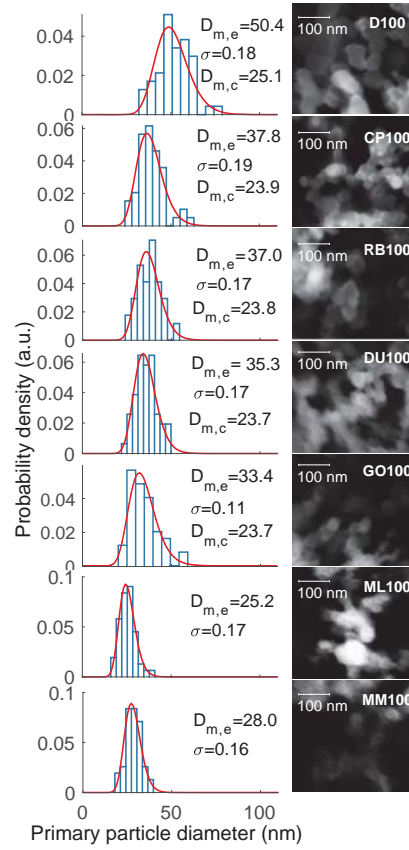


Figure 7: SEM images and corresponding particle size distribution for tested neat fuel cases. Best lognormal fit of the measured diameter distribution shown as red solid line. Best fit values of geometric mean diameter $D_{m,e}$ and distribution width σ are shown in the histogram for each case. The calculated mean particle diameter $D_{m,c}$ using the model described in Section 3 is also listed in the figure.

252 7. The primary particle size was modelled as a lognormal distribution, with
253 a best fit geometric mean diameter $D_{m,e}$, and distribution width σ , as ob-
254 tained from experiments, and shown in the histograms of tested cases. The
255 results indicate that the cases with higher f_v also yield larger $D_{m,e}$. The
256 calculated values obtained, $D_{m,c}$, are however, somewhat smaller than mea-
257 sured values. Experimentally measured number densities are estimated as
258 $N_p = 6f_v/\pi D_{m,e}^3$. The results show that not only do biofuels produce smaller
259 particle sizes, but also a smaller number of particulates compared to diesel.
260 For example, the $D_{m,e}$ derived mean particle volume in CP100 case is about
261 41% of D100 case, and the estimated \bar{f}_v are around 28% of D100. The es-
262 timated number density of soot particles in the case of biodiesels is 30% to
263 35% lower than that of D100, showing that the biofuels not only produce
264 smaller particle sizes, but also fewer particulates compared to diesel.

265 Among biofuels, the two most unsaturated fuels (CP and RB) produce
266 larger sizes and number densities of soot particles compared to the two less
267 saturated biofuels (DU and GO) and the two methyl esters (ML and MM).
268 This results from the fact that unsaturated bonds increase the concentration
269 of both soot inception and growth species such as benzene C_6H_6 and acetylene
270 C_2H_2 , which are believed to be the main soot surface growth species according
271 to the HACA mechanism [31]. Similar conclusions were also drawn in [7], in
272 which the fuel was diluted using N_2 .

273 As a whole, the soot model can effectively capture the reduction of soot
274 formation by adding biodiesel fuels. However, several discrepancies between
275 simulations and measurements arise, namely: for the pure diesel case, soot
276 value predictions are lower than those measured, and the soot also disappears

277 later than predicted. For biodiesels, the concentrations are lower and more
278 distributed, and the average primary particle size is smaller. The differences
279 can be attributed to the following reasons.

280 First, by approximating the ratio of carbon/hydrogen/oxygen, bond satura-
281 tion and heating values, we assumed input compositions of the diesel and
282 biodiesel fuels in the simulations (Tables 2 and 3). However, these are still
283 simplifications compared to the hundreds of hydrocarbons present. Second,
284 the chemical kinetic model [18] employed in this simulation is semi-detailed
285 for pyrolysis and combustion of the main substances of diesel and biodiesel
286 fuels.

287 However, many elementary chemical reactions are condensed into model
288 reactions, and the concentrations of the precursor species (PAHs, OH, C₂H₂)
289 used in soot modelling. Lastly, soot modelling relies on empirical paramete-
290 rs from the gas-phase chemistry by Blanquart *et al.* [34], which were in
291 turn calibrated based the measured soot morphology (average primary par-
292 ticle size) in ethylene diffusion flames [19], rather than the present biofuel or
293 liquid fuel flames. The soot model applied in this research proves to be rea-
294 sonable in dealing with sooting flames with different fuels, but is likely to be
295 more accurate by adjusting based on morphological parameters in the diesel
296 and biodiesel fuels individually. However, the precondition is that we have
297 sufficient knowledge to confirm the uncertainty of the chemical mechanism
298 or find more accurate but efficient chemical kinetics, because the community
299 have consensus that empirical parameters of soot models are dependent on
300 the flame type, fuel and the chemical mechanisms employed.

301 **5. Conclusions**

302 Soot volume fractions in undiluted, fully pre-vapourised, co-flow diffu-
303 sion diffusion flames fuelled with four real biodiesels, two methyl esters, and
304 their blends with petroleum diesel were measured using LII/extinction and
305 modelled using diffusion flame models including population balance and soot
306 kinetics. The maximum soot volume fraction ($f_{v,m}$) measured using neat
307 biodiesels cases is between 24.4% – 41.2% of the corresponding values in a
308 pure diesel flame (D100). SEM image analysis of samples shows that the
309 biodiesel combustion in co-flow diffusion flames produces smaller particle
310 sizes compared to the D100 case.

311 A comparison between soot production by biodiesel and methyl esters
312 shows that the unsaturation degree correlates positively with the sooting
313 propensity of fuels. Simulations have employed a population balance-based
314 soot model and a semi-detailed chemical mechanism. The results show
315 that the model can capture the reduction of soot formation by addition of
316 biodiesels, but not necessarily the rate of decrease with blending. Further
317 work is required to resolve discrepancies between numerical and experimental
318 results, especially in the case of D100.

319 **Acknowledgements**

320 Bo Tian is supported by the fellowship provided by ZEPI. C. T. Chong is
321 supported by the Newton Advanced Fellowship of the Royal Society (NA160115).
322 Anxiong Liu gratefully acknowledges the financial support of the Chinese
323 Scholarship Council (CSC) and the EPSRC grant No. EP/S012559/1.

324 **References**

- 325 [1] J. V. Gerpen. Biodiesel processing and production. *Fuel Processing*
326 *Technology*, 86(10):1097 – 1107, 2005. Biodiesel Processing and Produc-
327 tion.
- 328 [2] M. R. Kholghy, J. Weingarten, and M. J. Thomson. A study of the
329 effects of the ester moiety on soot formation and species concentrations
330 in a laminar coflow diffusion flame of a surrogate for B100 biodiesel.
331 *Proceedings of the Combustion Institute*, 35(1):905–912, 2015.
- 332 [3] M. K. Tran, D. Dunn-Rankin, and T. K. Pham. Characterizing sooting
333 propensity in biofuel-diesel flames. *Combustion and Flame*, 159(6):2181–
334 2191, 2012.
- 335 [4] S. K. Hoekman, A. Broch, C. Robbins, E. Cenicerros, and M. Natarajan.
336 Review of biodiesel composition, properties, and specifications. *Renew-*
337 *able and Sustainable Energy Reviews*, 16(1):143 – 169, 2012.
- 338 [5] J. Abboud, J. Schobing, G. Legros, J. Bonnety, V. Tschamber, A. Brill-
339 lard, G. Leyssens, V. Lauga, E. E. Iojoiu, and P. D. Costa. Impacts
340 of oxygenated compounds concentration on sooting propensities and
341 soot oxidative reactivity: Application to Diesel and Biodiesel surrogates.
342 *Fuel*, 193:241–253, 2017.
- 343 [6] Z. Gao, L. Zhu, X. Zou, C. Liu, B. Tian, and Z. Huang. Soot reduction
344 effects of dibutyl ether (DBE) addition to a biodiesel surrogate in lami-
345 nar coflow diffusion flames. *Proceedings of the Combustion Institute*, 37
346 (1):1265–1272, 2019.

- 347 [7] M. R. Kholghy, J. Weingarten, A. D. Sediako, J. Barba, M. Lapuerta,
348 and M. J. Thomson. Structural effects of biodiesel on soot formation in a
349 laminar coflow diffusion flame. *Proceedings of the Combustion Institute*,
350 36(1):1321–1328, 2017.
- 351 [8] W. Merchan-Merchan, S. McCollam, and J. F. C. Pugliese. Soot forma-
352 tion in diffusion oxygen-enhanced biodiesel flames. *Fuel*, 156:129–141,
353 2015.
- 354 [9] W. Merchan-Merchan, A. Abdihamzehkolaei, and D. A. Merchan-
355 Breuer. Formation and evolution of carbon particles in coflow diffusion
356 air flames of vaporized biodiesel, diesel and biodiesel-diesel blends. *Fuel*,
357 226(November 2017):263–277, 2018.
- 358 [10] R. Lemaire, S. Bejaoui, and E. Therssen. Study of soot formation during
359 the combustion of Diesel, rapeseed methyl ester and their surrogates in
360 turbulent spray flames. *Fuel*, 107:147–161, 2013.
- 361 [11] Dhrubajyoti D. Das, Charles S. McEnally, and Lisa D. Pfefferle. Sooting
362 tendencies of unsaturated esters in nonpremixed flames. *Combustion and
363 Flame*, 162(4):1489–1497, 2015.
- 364 [12] C. T. Chong, B. Tian, Han N-J, L. Fan, S. Ni, K. Wong, and
365 S. Hochgreb. Quantification of carbon particulates produced under
366 open liquid pool and prevaporised flame conditions: Waste cooking oil
367 biodiesel and diesel blends. *Fuel*, 270, 2020. doi: 10.1016/j.fuel.2020.
368 117469.

- 369 [13] C. T. Chong and S. Hochgreb. Spray combustion characteristics of
370 palm biodiesel. *Combustion Science and Technology*, 184(7-8):1093–
371 1107, 2012.
- 372 [14] M. Matti Maricq. Physical and chemical comparison of soot in hydrocar-
373 bon and biodiesel fuel diffusion flames: A study of model and commercial
374 fuels. *Combustion and Flame*, 158(1):105–116, 2011.
- 375 [15] B. Tian, Y. Gao, C. Zhang, and S. Hochgreb. Soot measurement by
376 combining continuous wave multipass extinction and laser-induced in-
377 candescence in diluted methane flames. *Combustion and Flame*, 192:
378 224–237, 2018.
- 379 [16] B. Tian, Y. Gao, S. Balusamy, and S. Hochgreb. High Spatial Resolution
380 Laser Cavity Extinction and Laser Induced Incandescence in Low Soot
381 Producing Flames. *Applied Physics B*, 120(3):469–487, 2015.
- 382 [17] B. Tian, C.T. Chong, L. Fan, J.-H. Ng, C. Zhang, and S. Hochgreb.
383 Soot volume fraction measurements over laminar pool flames of biofuels,
384 diesel and blends. *Proceedings of the Combustion Institute*, 37(1):877–
385 884, 2018.
- 386 [18] E. Ranzi, A. Frassoldati, R. Grana, A. Cuoci, T. Faravelli, A. P. Kel-
387 ley, and C. K. Law. Hierarchical and comparative kinetic modeling of
388 laminar flame speeds of hydrocarbon and oxygenated fuels. *Progress in*
389 *Energy and Combustion Science*, 38(4):468–501, 2012.
- 390 [19] Anxiong Liu and Stelios Rigopoulos. A conservative method for numer-

- 391 ical solution of the population balance equation, and application to soot
392 formation. *Combustion and Flame*, 205:506–521, 2019.
- 393 [20] J. Yon, R. Lemaire, E. Therssen, P. Desgroux, A. Coppalle, and K. F.
394 Ren. Examination of wavelength dependent soot optical properties of
395 diesel and diesel/rapeseed methyl ester mixture by extinction spectra
396 analysis and LII measurements. *Applied Physics B*, 104(2):253–271,
397 2011.
- 398 [21] P. K. Sahoo, L. M. Das, M. K.G. Babu, P. Arora, V. P. Singh, N. R.
399 Kumar, and T. S. Varyani. Comparative evaluation of performance and
400 emission characteristics of jatropha, karanja and polanga based biodiesel
401 as fuel in a tractor engine. *Fuel*, 88(9):1698–1707, 2009.
- 402 [22] M. Chhabra, A. Sharma, and G. Dwivedi. Performance evaluation of
403 diesel engine using rice bran biodiesel. *Egyptian Journal of Petroleum*,
404 26(2):511–518, 2017.
- 405 [23] A. Probudha Hasan, A. Wakil, and A. Kafy. Prospect of rice bran for
406 biodiesel production in Bangladesh. *Procedia Engineering*, 90(December
407 2014):746–752, 2014.
- 408 [24] NIST. Chemistry webbook, srd 69, dodecanoic acid, methyl ester.
409 <https://webbook.nist.gov/cgi/cbook.cgi?ID=111-82-0>, 2018. Ac-
410 cessed: 2019-03-10.
- 411 [25] NIST. Chemistry webbook, srd 69, methyl tetradecanoate n.d. <https://webbook.nist.gov/cgi/cbook.cgi?ID=C124107&Mask=4>, 2018. Ac-
412 cessed: 2019-03-10.
413

- 414 [26] Y. Ying and D. Liu. Effects of butanol isomers additions on soot nanos-
415 tructure and reactivity in normal and inverse ethylene diffusion flames.
416 *Fuel*, 205:109–129, 2017.
- 417 [27] J. Duan, Y. Ying, and D. Liu. Novel nanoscale control on soot formation
418 by local CO₂ micro-injection in ethylene inverse diffusion flames. *Energy*,
419 179:697–708, 2019.
- 420 [28] A. Frassoldati, A. Cuoci, A. Stagni, T. Faravelli, and E. Ranzi. Skele-
421 tal kinetic mechanism for diesel combustion. *Combustion Theory and*
422 *Modelling*, 21(1):79–92, 2017.
- 423 [29] Y. Ra and R. D. Reitz. A combustion model for IC engine combustion
424 simulations with multi-component fuels. *Combustion and Flame*, 158
425 (1):69–90, 2011.
- 426 [30] A. Li, L. Zhu, Y. Mao, J. Zhai, D. Han, X. Lu, and Z. Huang. Surrogate
427 formulation methodology for biodiesel based on chemical deconstruction
428 in consideration of molecular structure and engine combustion factors.
429 *Combustion and Flame*, 199:152–167, 2019.
- 430 [31] Michael Frenklach. Reaction mechanism of soot formation in flames.
431 *Physical Chemistry Chemical Physics*, 4(11):2028–2037, 2002.
- 432 [32] H. Bockhorn, A. D’Anna, A. F. Sarofi, and H. Wang. A joint volume-
433 surface-hydrogen multi-variate model for soot formation. In *Combustion*
434 *Generated Fine Carbonaceous Particles*, pages 437–463. KIT Scientifi
435 Publishing, Karlsruhe, 2009.

- 436 [33] Srinivas Vemury and Sotiris E. Pratsinis. Self-preserving size distribu-
437 tions of agglomerates. *Journal of Aerosol Science*, 26(2):175–185, 1995.
- 438 [34] G. Blanquart, P. Pepiot-Desjardins, and H. Pitsch. Chemical mechanism
439 for high temperature combustion of engine relevant fuels with emphasis
440 on soot precursors. *Combustion and Flame*, 156(1):588–607, 2009.
- 441 [35] P. Pepiot-Desjardins, H. Pitsch, R. Malhotra, S. R. Kirby, and A. L.
442 Boehman. Structural group analysis for soot reduction tendency of oxy-
443 genated fuels. *Combustion and Flame*, 154(1-2):191–205, 2008.